Accepted Manuscript

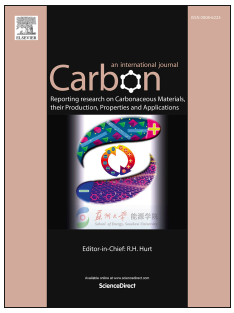

Tough and conductive hybrid graphene-PVA: Alginate fibrous scaffolds for engineering neural construct

Nasim Golafshan, Mahshid Kharaziha, Mohammadhossein Fathi

PII: S0008-6223(16)30904-6

DOI: 10.1016/j.carbon.2016.10.042

Reference: CARBON 11401

To appear in: *Carbon*

Received Date: 21 August 2016

Revised Date: 23 September 2016

Accepted Date: 18 October 2016

Please cite this article as: N. Golafshan, M. Kharaziha, M. Fathi, Tough and conductive hybrid graphene-PVA: Alginate fibrous scaffolds for engineering neural construct, *Carbon* (2016), doi: 10.1016/j.carbon.2016.10.042.

This is a PDF file of an unedited manuscript that has been accepted for publication. As a service to our customers we are providing this early version of the manuscript. The manuscript will undergo copyediting, typesetting, and review of the resulting proof before it is published in its final form. Please note that during the production process errors may be discovered which could affect the content, and all legal disclaimers that apply to the journal pertain.

ACCEPTED MANUSCRIPT

Tough and conductive hybrid Graphene-PVA: Alginate fibrous scaffolds for engineering neural construct

Nasim Golafshan[1], Mahshid Kharaziha[1*], Mohammadhossein Fathi[1]

1. Department of Materials Engineering, Isfahan University of Technology, Isfahan 84156-83111, Iran

* **Corresponding author e-mail**: ma.kharaziha@gmail.com

Abstract

The aim of this study was to develop a hybrid Gr nanosheets-sodium alginate (SA)/polyvinyl alcohol (PVA) (Gr-AP) fibrous scaffold with exceptional toughness and electrical conductivity for nerve tissue engineering. Furthermore, the effects of Gr concentration (0, 0.5, 1, 2 and 5 wt.%) on the electrical, mechanical, physical and biological properties as well as degradation date of scaffolds were evaluated. Results demonstrated that, compared to AP scaffold, the toughness of hybrid Gr-AP scaffold containing 1 wt.% Gr considerably improved (4-fold) which attributed to the strong interfacial interactions between Gr nanosheets and AP matrix. Furthermore, 1wt.% Gr in AP scaffolds acted as electrical nanobridges leading to improved electrical conductivity of the pure AP scaffold. To estimate cell response dependence on the substrate properties, the PC12 cells were cultured on Gr-AP scaffolds. Results revealed the potentials of Gr content scaffolds to support attachment and spreading of PC12 cells. Moreover, MTT assay also confirmed that after 7 days of culture, the hybrid scaffold consisting of 1wt.% Gr nanosheets significantly promoted cell proliferation compared to AP scaffold (1.4-fold). Overall, our findings demonstrated that Gr-AP scaffolds exhibited superior electrical and mechanical properties with enhanced PC12 cell interaction. It is envisioned that the offered hybrid Gr-AP scaffolds might have great potential to develop the devices for peripheral nerve regeneration. However, further biological studies along with electrical stimulation are necessary to evaluate the role of hybrid Gr-AP scaffolds on the nerve regeneration.

Keywords: Peripheral nerve tissue engineering; Graphene; Electrospinning; Interpenetrating network; Conductivity; Toughness.

Introduction

Painful peripheral nerve injuries denote a substantial challenge for reconstructive surgeries due to long-term disability and poor operative effects. Normally, axon extensions could regenerate the small gaps triggered by injury, recombining with the distal stump and ultimately reestablishing its function [1, 2]. If the considerable loss of nervous tissue occurs, clinical treatment consisting of donor nerves obtained from a second operative site of the patient, such as vein or arterial graft, is an unmet need. Due to the potential formation of painful neuromas, structural differences between donor and recipient grafts preventing from a successful regeneration, and shortage of graft material for extensive repair, this method is far from being the gold standard [3]. Recent progresses in tissue engineering have paved the way to create artificial nerve grafts with appropriate physiological properties for peripheral nerve [4].

In order to fabricate fully functional and biomimetic nerve substitutes, various kinds of polymeric-based scaffolds have been proposed [5]. Artificial nerve grafts need to structurally and mechanically mimic the native extracellular matrix (ECM) in order to provide the correct environment for the neotissues [6]. To simulate the native nerve tissue, the scaffolds should present appropriate mechanical characteristics while providing sufficient flexibility [7]. Furthermore, artificial nerve grafts need to be electric conductance to support the electrical conduction of injured nerve during regeneration and enhance regeneration by accelerating axonal elongation on the charged surface [8]. To date, numerous studies have focused on the simulation of the natural ECM thorough the development of fibrous constructs using self-assembly [9], template-directed synthesis [10], phase separation [11], and electrospinning [12] approaches. Between them, electrospinning technique has been extensively accepted as the simplest and least expensive technique in the fabrication of highly porous micro- and nanofibrous scaffolds comprised of interconnected pores to simulate the architecture of natural ECM [13].

So far, various types of natural and synthetic polymeric biomaterials have been utilized in order to develop physiologically relevant scaffolds for peripheral nerve tissue engineering applications [4]. An appropriate biomaterial needs to induce appropriate chemical and physical signaling cues which transduce into intracellular biochemical responses to moderate the cellular function [4]. For instance, alginate which is a negatively charged polysaccharide derived from

brown seaweed, has been widely applied to develop artificial constructs for peripheral nerve tissues [14]. It gains negative charge due to the carboxyl groups placed on the ring structure of both β-D mannuronate (M block) and α-L guluronate (G) monomers [15]. Alginate has prominent characteristics such as non-toxicity, biodegradability and biocompatibility making it a suitable material for nerve tissue engineering applications [8]. However, aqueous alginate solutions are too viscous to be electrospun into fiber forms. Furthermore, alginate based scaffolds often lack the mechanical strength to help rigorous physiological loading conditions [16] and reveal high degradation rate [17] leading to the combination of alginate with other types of synthetic polymers such as polycaprolactone (PCL) [16], polyacrylamide [18] and polyvinyl alcohol (PVA) [19], with higher mechanical properties and slower degradation kinetics. In other words, PVA is a water-soluble polymer with good spinnability and biocompatibility which has been widely applied to develop fibrous constructs for engineering various tissues such as nerve [20, 21], heart [22] and vascular system [15]. For example, PVA fibrous scaffold with average fiber diameter of 410-1062 nm was developed using electrospinning for neural tissue engineering [21]. Results demonstrated the positive role of PVA fibers on the adhesion, proliferation, migration, and differentiation of PC12 cells. However, the lack of antigenicity and weak cell affinity limited the pure application of synthetic polymers [4, 23]. It is envisioned that through the development of interpenetrating network (IPN) and semi-IPN constructs, it would be possible to develop biomaterial-based constructs with suitable characteristics for growth and maturation of nerve cells [22, 24, 25]. This network could provide supreme mechanical strength and toughness when one polymer component cross-linked covalently and the other cross-linked ionically [24]. In this way, PVA and alginate have recently blended to make IPN and semi-IPN constructs [22, 26].

Despite the promising results, the most of the previously reported scaffolds are electrically insulating at biologically relevant frequencies. To further enhance the electrical and mechanical characteristics of the scaffolds, a number of researches have focused on the incorporation of conductive nanomaterials such as polypyrrole [27], silver [28], gold [29], carbon nanotubes (CNTs) [30] and graphene (Gr) [31] within polymeric matrices to improve material-neuron interaction via supporting and encouraging the neural regeneration following the damage [30]. In particular, Gr, a monolayer of carbon atoms arranged in a two dimensional (2D) honeycomb

lattice, has glimmered great interest of researchers due to its excellent mechanical, electrical, thermal and optical properties, and ultrahigh specific surface area [32]. Remarkable physicochemical characteristics of Gr as well as its biocompatibility motivated scientists to employ this material for tissue regeneration [31]. For instance, it was demonstrated that three-dimensional Gr foams (3D-GFs) could not only support neural stem cell growth, but also preserve the cell at the active proliferation state [33]. Recently, Gr was employed to improve the mechanical properties of PVA[34, 35] or alginate [36]-based scaffolds for tissue engineering. Despite improved mechanical and electrical characteristics, Gr-incorporated polymeric scaffolds did not reveal desired toughness and architectural complexities suitable for nerve tissue engineering.

In this work, we developed hybrid Gr incorporated alginate/PVA (Gr-AP) fibrous scaffolds with a wide range of composition using electrospinning approach for engineering nerve tissue. We also investigated the effect of Gr content on the mechanical, structural, chemical, electrical and biological properties of hybrid fibrous scaffolds. It is hypothesized that the development of an electrical conductive and flexible nanofibrous scaffold could simultaneously induce mechanical and electrical cues to support nerve cell functions.

Materials and methods

2.1. Materials

Alginic acid sodium salt (SA) from brown algae (medium viscosity), PVA (Mw=72,000) and Triton X-100^{TM} were provided from Sigma-Aldrich and Merck Co, respectively. Pristine graphene (less than 32 Layers, purity > 99.5%) purchased from Nanosany Corporation. Glycerol and $CaCl_2$ was obtained from Merck Co. Double distilled (DI) water was used in all the sections of experiment.

2.2. Fabrication of hybrid Gr-AP scaffolds

Hybrid Gr-AP fibrous scaffolds with various concentrations of Gr were prepared using electrospinning technique. Primarily, the SA and PVA aqueous solutions in DI water with concentrations of 4 wt.% and 8 wt.%, respectively, were prepared, separately. In order to

overcome the high viscosity of SA in aqueous solution, 51 wt.% glycerol aqueous solution was added to SA solution (glycerol: DI water volume ratio 3:4). Consequently, the SA and PVA aqueous solutions were mixed to get a homogenous solution. The volume ratio of SA:PVA solutions was selected according to the primarily study on the effects of various volume ratios of Alginate:PVA (10:90, 20:80, 30:70 and 40:60) on the electrospinability of mixture and structural properties of AP scaffolds. To obtain various concentrations of Gr embedded polymer suspensions (0, 0.5, 1, 2 and 5 wt.%), Gr nanosheets dispersed in DI water using 30 min sonication was added to AP solution and stirred for a day at ambient temperature in order to prepare final homogenous suspensions. Before electrospinning process, Triton X100 at the concentration of 0.5 wt.% was added to the suspensions to improve their spinability. Finally, polymer suspensions were sonicated for 30 min (WUD-D10H, Power 770 W) at room temperature to provide a homogenous dispersion of Gr nanosheets.

To develop the intended hybrid scaffolds, as prepared suspensions, which was fed into 1 mL syringe having a 23G blunted stainless steel needle was electrospun (Fig. 1(A)). During the electrospinning process, voltage, flow rate and the tip to the collector distance were set to 18 kV, 0.12 mL/h and 15 cm, respectively. A grounded aluminum foil was used as a collector to create the electrospun fibrous scaffolds. Upon electrospinning, the fabricated scaffolds were dried in a vacuum desiccator at room temperature prior to crosslinking and further characterizations. Crosslinking process was performed in two steps of covalently and ionically in order to crosslink PVA and alginate polymers, respectively. While heat treatment process and methanol soaking were used to crosslink PVA, $CaCl_2$ solution was applied to ionically crosslink SA. Primarily, the scaffolds were kept in 80 °C for 24 h, and then, immersed in pure methanol solution for 1 h. In the next step, the scaffolds were ionically crosslinked in 2 wt.% $CaCl_2$ solution for 1 h at ambient temperature. After the crosslinking process, uncrosslinked polymers were removed by rinsing the scaffolds phosphate buffered saline (PBS) solution.

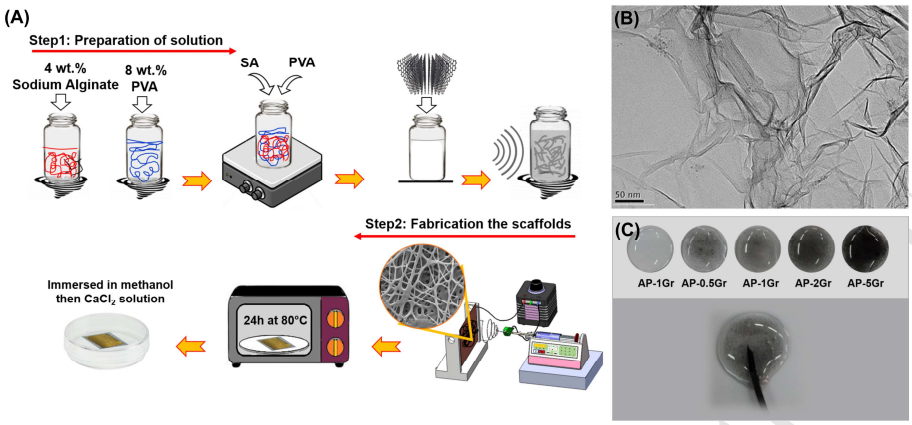

Fig. 1. A) Schematic diagram describing the fabrication of Gr-AP fibrous scaffold consisting of two steps: preparation of precursor solution (step 1), fabrication and crosslinking of the scaffolds (step 2). Crosslinking process consisted of two steps in which PVA and alginate were crosslinked, consequently. B) TEM image of Gr nanosheet. C) Optical images of AP solutions with various concentrations of Gr nanosheets (0, 0.5, 1, 2 and 5 wt.%).

2.3. Characterizations of hybrid Gr-AP scaffolds

The surface morphology of prepared scaffolds, before and after crosslinking process, was studied by scanning electron microscope (SEM, Philips, XL30). Before imaging, the samples were sputter coated with a thin layer of gold. The fiber size of the electrospun scaffolds was also determined (n=30) using SEM images along with NIH Image J software. Moreover, the Gr distribution within the fibrous scaffolds was assessed using transmission electron microscope (TEM) (Philips EM208S 100 kV) on the samples directly deposited on the carbon coated copper grid.

The chemical composition of the prepared scaffolds was verified through Attenuated total reflectance-Fourier transform infrared spectroscopy (ATR-FTIR, Bruker tensor), performed over a range of 600-3700 cm^{-1} and resolution of 2 cm^{-1} and X-ray diffraction (XRD, X' Pert Pro X-ray diffractometer, Phillips, Netherlands), carried out with CuKa radiation (λ=0.154 nm) at a generator voltage of 40 kV and a current of 40 mA. Furthermore, The functional groups on the surface of Gr nanosheets as well as Gr-AP fibrous scaffold were identified using a Senterra Raman spectroscope (Bruker, Germany) equipped with a 785 nm laser.

The wettability and hydrophilicity of the scaffolds (n =3) were evaluated via water contact

angle measurement with a Drop Shape Analysis System (Sessile Drop, G10) on the crosslinked scaffolds. 4µL water droplet was applied in the measurements and the contact angle between the drop and the scaffolds was subsequently measured. More than five measurements on different locations of the scaffold surfaces were conducted for each group of the sample and the contact angle was measured at the first seconds of falling a drop on scaffolds. Finally, the average contact angle with standard deviation (SD) was reported.

Moreover, *in vitro* degradation assay was applied to determine the weight loss of the crosslinked scaffolds. Three samples of each type of different scaffolds with weight of about 2 mg were incubated in PBS at 37 °C for 1, 7, 14, 21 and 28 days, where the pH was near identical to the physiological conditions (PH=7.4). PBS was refreshed every three days. At time point, the samples were rinsed with PBS, dried and weighted. Finally, the degradation percentage was estimated via dividing the weight loss by the initial dry weight.

Electrical impedance analysis was applied in order to evaluate the electrical properties of the scaffolds (length: 20 mm, width: 20 mm, thickness: 0.15 mm) (n=3) using PARSTAT 2273, USA electrochemical work-station. Electrochemical measurements were performed in 2 M H_2SO_4 electrolyte at room temperature using three-electrode system consisting of a Ag/AgCl as the reference electrode, a platinum electrode as counter electrode, and the scaffolds put on glass slides as working electrode. a.c. bias was swept over a frequency range from 10 Hz to 1.0 MHz and the impedance was subsequently recorded at each frequency. Moreover, the electrical conductance of polymeric solution was measured by JENWAY 4520 at room temperature.

Mechanical properties of electrospun scaffolds were determined using a tensile tester (Hounsfield H25KS) with a load cell capacity of 10 N at 5 mm/min rate. Before mechanical testing, the specimens in the shape of rectangular and with dimension of 10 mm×10 mm and average thickness of 200 µm were immersed in PBS for 1 day. After plotting the stress-strain curves (n=5), the mechanical properties consisting of energy per volume (toughness), strain at break (elongation), tensile strength and modulus were calculated. The tensile modulus was calculated from the initial 0-10% of linear region of the stress-strain curves while the energy per volume was measured from the area under the stress-strain curves after plastic deformation (toughness).

2.4. Cell culture

The PC12 cell line obtained from Pasteur Institute of Iran (NCBI code: C153) was cultured in Dulbecco's modified Eagle medium (DMEM, Bioidea, Iran) supplemented with 10% (v/v) horse serum (HS, Bioidea, Iran), 5% (v/v) fetal bovine serum (FBS, Bioidea, Iran), and 1% (v/v) penicillin/streptomycin (pen/strep, Bioidea, Iran) at 37 °C in a humidified atmosphere containing 5% CO2. The culture medium was changed every 2 days. Before cell seeding, fibrous scaffolds on glass slides were placed in a 24-well plate, washed thrice with PBS and sterilized for 30 min in 70% (v/v) ethanol and 2 h under UV light. The scaffolds were then immersed in the culture medium consisting of DMEM containing 10% (v/v) FBS and 1% (v/v) pen/strep) for overnight prior to cell seeding. After reaching 70-80% confluency, the cells were detached with 0.25% trypsin/EDTA solution (Bioidea, Iran) and counted by trypan blue assay. Finally, they were collected from the flask, counted and seeded on the samples (n=3) as well as tissue culture plate (TCP) (control) with a density of 10^4 cells/well. Cells were incubated at 37 °C under 5%CO_2 condition for 7 days and medium was changed every three days.

2.4.1. Cell viability study

The relative viability of cells was studied by 3-(4,5-dimethylthiazolyl-2)-2,5-diphenyl tetrazolium bromide (MTT) gained from Sigma-Aldrich colorimetric assay. At the predicted time of 1, 4 and 7 days of incubation, culture medium was discarded, the wells were washed with PBS and the samples as well as controls (n=3 per group) were incubated with MTT solution (0.5 mg/ml MTT reagent in PBS) for 4 h. The dark blue formazan crystals were solubilized with the MTT solvent (dimethyl sulfoxide (DMSO)) and kept for 1 h at 37 °C on shaker. Subsequently, 100 µL of dissolved formazan solution of each sample was moved to 96-well plate and the optical density (OD) of each well was measured with a microplate reader (Bio Rad, Model 680 Instruments) against DMSO (blank) at a wavelength of 540 nm and a reference filter of 630 nm. The percent of cell survival was calculated based on the following equation (Equation 1):

$$\textit{Relative cell viability}\ (\%) \quad \frac{A_{sample} \quad A_b}{A_c \quad A_b} \times 100 \qquad (1)$$

where A_{sample}, A_b and A_c were absorbance of sample, blank (TCP) and control (DMSO), respectively.

2.4.2. Cell attachment and morphology study by SEM observation

The attachment and morphology of the cells seeded on the scaffolds were evaluated by SEM analysis. After fixation with 2.5%(v/v) glutaraldehyde (sigma) for 3 h, the samples were rinsed with PBS, and dehydrated in the graded concentrations of ethanol (30, 70, 90, 96 and 100% v/v) for 10 min, respectively. Finally, they were air dried, gold-coated and evaluated via observing by SEM. To determine the cell spreading over culture time, two samples of each condition were selected, ten random images for each sample were taken and the proportion of area covered by cell at each μm^2 of the samples was calculated using image J software (1.51V).

2.5. Statistical analysis

The data in this study were analyzed using one-way ANOVA analyses and reported as mean ± standard deviation (SD). To determine a statistically significance difference between groups, Tukey's post-hoc test using GraphPad Prism Software (V.6) with a p-value <0.05 was applied to be significant.

3. Results and discussion

3.1. Fabrication and characterization of the hybrid nanofibrous scaffolds

The peripheral nerve ECM consists of the collagen based fibrous substrate providing a proper microenvironment to support the Schwann cell function [37]. In order to mimic the peripheral nerve ECM, hybrid Gr-AP fibrous scaffolds were fabricated using electrospinning technique. Prior to Gr nanosheet incorporation, the amount of alginate and PVA polymers was modulated in order to develop the scaffold with uniform architecture and appropriate fiber and pore size (supplementary Fig. S1). Fig. S1 shows the SEM images of AP fibrous scaffolds consisting of various amount of alginate (40, 30, 20 and 10 v/v%). PVA-40%Alginate fibrous scaffold (A6P) consisted of thick fibers, which densely fused together leading to significantly reduced pore size (547±42 nm). Increasing the PVA content resulted in less fiber fusion and more homogenous

pores. Moreover, the average fiber diameter of scaffolds (Fig. S1(E)) reduced with increasing PVA content due to the excellent spinnability of PVA ($p<0.05$). Addition of PVA to alginate solution resulted in reduced surface tension and viscosity of SA solution leading to reduce in fiber size of scaffolds. Due to formation of scaffolds consisting of uniform architecture and smooth fibers with appropriate sizes, the Alginate:PVA mixture consisting of SA:PVA = 20:80 volume ratio was selected for further experiments. Consequently, Gr nanosheets with the thickness of 2-18 nm and diameter of 4-12 µm (Fig. 1(B)) were incorporation within AP solution to develop hybrid Gr-AP fibrous scaffolds containing various amounts of Gr content (0, 0.5, 1, 2 and 5 wt.%). The color of Gr-AP suspensions was observed to be darker with increasing Gr content from 0 to 5 wt.%. (Fig. 1(C)). Furthermore, Gr-AP suspensions revealed uniform black color in which no sign of aggregation could be observed suggesting a homogenous distribution of Gr within the polymer solution.

After electrospinning process, since both PVA and alginate are water soluble, crosslinking was performed to stabilize the scaffold structures. The scaffolds were crosslinked via a two-step process without using any cytotoxic material ($CaCl_2$, methanol and heat-treatment) (Fig. 1(A)). SEM images revealed the successful development of as-electrospun (Figs. 2(A, B) and supplementary Fig. S2) and crosslinked (Figs. 2(C, D) and supplementary Fig. S2) scaffolds with greatly uniform and random fibers and interconnected porous structure. Addition of Gr nanosheets did not significantly change the morphology of the fibers confirming the incorporation of Gr nanosheets within the fibers. TEM image of 1Gr-AP scaffold (Fig. 2(E)) could also demonstrate that Gr nanosheets were uniformly distributed within the AP nanofibers (404±24 nm) without any agglomeration. TEM image with higher magnification of 1Gr-AP scaffold (insets in Fig. 2(E)) also revealed the presence of Gr nanosheets with size of 88±13 nm confirming the mono-dispersion of Gr nanosheets within the AP matrix. Previous results revealed the formation of bead-like defects along the electrospun PVA fibers due to the aggregation of GO nanosheets at above 3 wt.% [38]. Our results revealed that these defect types did not form confirming the uniform distribution of Gr nanosheets up to 5 wt.%. Furthermore, all fibrous scaffolds specifically pure AP one, consisted of some junctions among the fibers leading to the adherence between fibers. It could be due to the trace remaining solvent after electrospinning due to high water binding capacity of alginate [39]. However, increasing Gr

content resulted in reduced water absorption leading to the reduction of junction points between fibers.

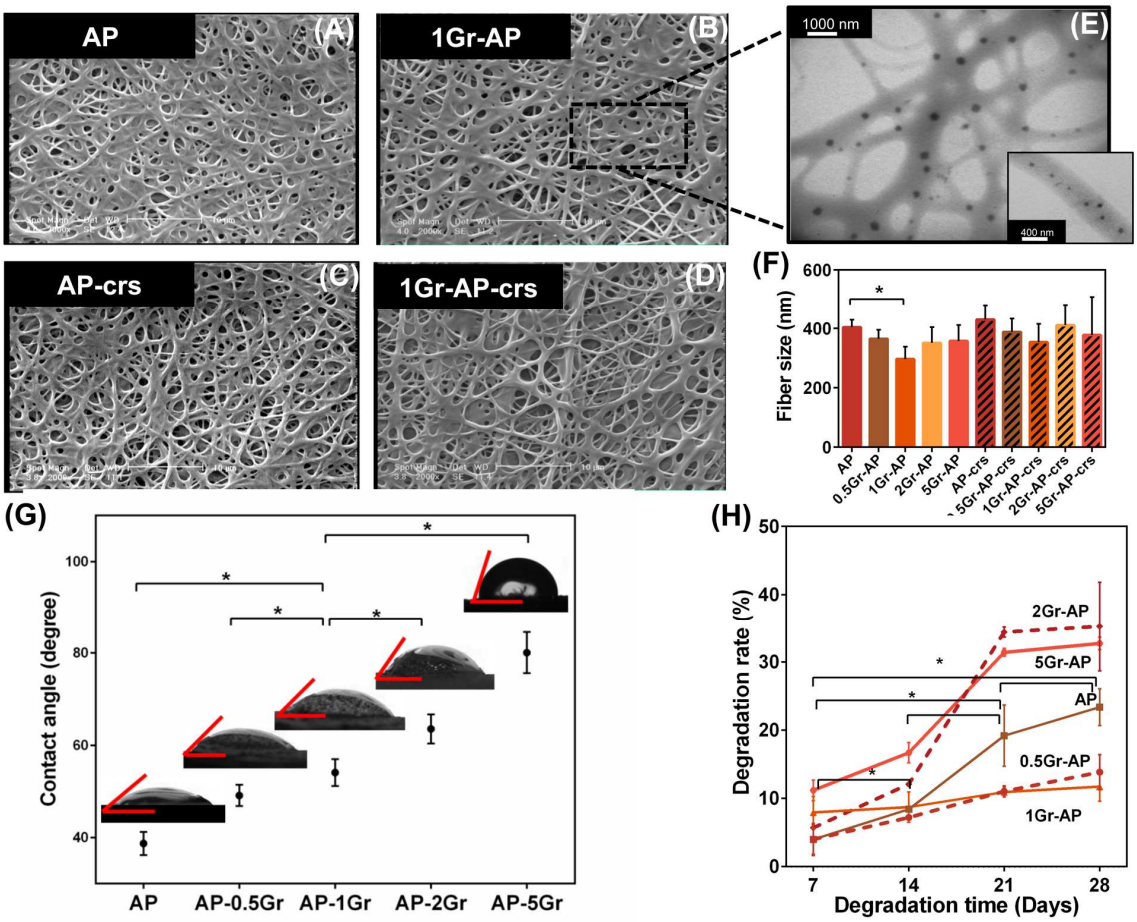

Fig. 2. Structural and chemical properties of hybrid scaffolds; SEM images of (A, C) AP and (B, D) 1Gr-AP fibrous scaffold, before (A and B) and after (C, D) crosslinking. E) TEM image of 1Gr-AP scaffolds. Magnified image shows the well distribution of Gr nanosheets within the fibrous structure. (F) Incorporation of Gr nanosheets significantly changed the average fiber size of scaffolds, before and after crosslinking process. (. "crs" was used for crosslinked samples.) G) Incorporation of Gr nanosheets also enhanced the water contact angle and, hence, hydrophobicity of scaffolds. H) The changes of degradation rate also revealed the crucial role of Gr nanosheet content on the degradation rate of scaffolds. (* $P < 0.05$).

Based on analyzing the SEM images, the average fiber diameter of the scaffolds reduced with increasing Gr content upon 1 wt. % (1Gr-AP scaffold) and then partially enhanced (Fig. 2(F)). Before crosslinking process, the average fiber size of 1Gr-AP scaffold was in the range of 296±40 nm, which was significantly smaller than that of pure AP scaffold (404±24 nm) ($P<0.05$). The intrinsic properties of polymeric solutions such as electrical conductivity and

polymer concentration can firmly affect the electrospinning process and forming the fibers [40]. The smaller fiber sizes of the Gr incorporated scaffolds could be the result of higher conductivity of the precursor suspension (Supplementary Table S1). The conductivity of the polymeric suspensions provided a stronger electrical force in the electrospinning process leading to the enhanced elongation and decreased fiber size [41]. While the conductivity of PVA solution was the lowest (247±20 µS), the conductivity of suspensions remarkably enhanced after blending with alginate (572±13 µS) which could be due to its anionic nature of alginate in water. Gr nanosheets were further affected the conductivity of AP solution due to its negative functional groups formed on the edge of nanosheets and leading to dramatically enhanced conductivity of suspensions up to 800±17 µS (at 1Gr-AP precursor solution). The previous literatures also demonstrated that the enhancement of conductivity with increasing Gr nanosheets [32, 42]. However, our data displayed that the addition of more Gr nanosheets (> 1 wt.%) resulted in reduced electrical conductance which might be due to percolation phenomenon [43]. Based on this phenomenon, in the nanocomposite materials, there is a critical concentration of filler in which filler-matrix and filler-filler interactions are in a balance statue. At this point named as percolation threshold, coagulation of filler results in development of a network which facile electron transfer in the matrix [43]. Based on our results, 0.5 wt.% Gr nanosheets is the percolation threshold in which addition of a bit more Gr nanosheets results in enhanced conductivity.

SEM images of the prepared scaffolds after crosslinking process (Figs. 2(C, D) and Supplementary Fig. S2) also obviously proved that crosslinking process resulted in larger and curled fibers, which were bonded together at numerous junctions. Specifically, the average fiber size of 0.5Gr-AP scaffold dramatically increased by 1.2 times from 365±25 nm to 388±25 nm which could be due to the swelling of the fibers through the crosslinking process. Additionally, similar to uncrosslinked step, the fiber sizes of scaffolds significantly ($P < 0.05$) decreased while Gr content increased upon 1 wt.% and then enhanced with increasing Gr content to above 5 wt.% (Fig. 2(D)).

Water contact angle test was applied to investigate the hydrophobicity level of the scaffolds (Fig. 2(G)). Due to the hydrophilic nature, electrospun AP scaffold revealed low water contact angle (40°±2), despite the crosslinking process. Water contact angle significantly enhanced with

increasing Gr nanosheets content ($P<0.05$) demonstrating superior hydrophobicity. For instance, water contact angle significantly increased to 82°±3 in 5Gr-AP scaffold. This result similarly reported in Gr incorporated PVA scaffold and recommended the effective role of Gr nanosheets on the water permeability [44]. Moreover, there was significant difference between the hydrophilicity of the membrane with various Gr contents which could be due to the presence of Gr that is improved the hydrophobia of the membrane.

One of the most crucial features of hydrophilic-based scaffolds is high degradation rate which considerably declines the mechanical characteristics during tissue regeneration. As illustrated in Fig. 2(H), the degradation profiles of Gr-AP scaffolds with different Gr nanosheet concentrations were similar to that of AP one. However, the incorporation of Gr nanosheets upon 1 wt.% within AP scaffold resulted in a statistically decrease in the degradation rate from 23.3 ±2.6 (for AP scaffold) to 13.8 ±2.5 (for 0.5Gr-AP) and 11.7±2.1%. (for 1Gr-AP). It might be due to strong interaction between Gr nanosheets and AP networks which able to bridge the cleaved PVA-alginate chains leading to delay in the scaffold degradation. This behavior was similarly reported for methacrylated GO-methacrylated gelatin (GelMA) hybrid hydrogel [45]. However, more increasing Gr nanosheets resulted in significantly enhanced degradation rate ($P<0.05$). It might be due to the agglomeration of Gr nanosheets leading to the weak interaction between Gr nanosheets and AP network, rapid degradation of polymer network and, hence, release of Gr nanosheets.

FTIR spectra of scaffolds, before (Supplementary Fig. S3(A)) and after (Fig. 3(A)) crosslinking process confirmed the formation of hydrogen bonding between Gr nanosheets and polymeric matrices after two-step crosslinking process. Before crosslinking process, PVA (Supplementary Fig. S3) consisted of the characteristic absorption peaks at 1427, 1370, 1325, 1250, 1090, and 840 cm^{-1} attributed to the (CH–OH), (CH–OH), (CH), (C–O), and (C–C) resonance, respectively [46]. After thermal and methanol crosslinking process (Fig. 3(A)), the C-H stretching vibration band at 2930 cm^{-1} related to CH_2 removed and a new peak at 1670 cm^{-1} corresponded to C=C appeared demonstrating the crosslinking of PVA [47]. In other words, before crosslinking process (Supplementary Fig. S3(A)) SA consisted of the characteristic bands of OH (at 3430 cm^{-1} and 850 cm^{-1}), asymmetric and symmetric COO (at 1620 cm^{-1} and 1415 cm^{-1}), C-O (at 1064 cm^{-1}), C-C (at 1036 cm^{-1}) and C-O-C (at 924 cm^{-1}) [26]. After ionically

crosslinking process with solution 2 wt.% $CaCl_2$ (Fig. 3(A)), calcium ions substituted sodium in SA structure resulted in the modulation of charge density, radius and atomic weight of the cations and hence shifting the asymmetric stretching vibration of carboxylate ion to lower wave numbers. Furthermore, the contribution of hydroxyl and carboxylate groups of alginate to the calcium ion to develop chelating structure and consequent reduce hydrogen bonding between hydroxyl functional groups affording narrower band in calcium alginate (924, 1077 and 1250 cm^{-1}). After semi-IPN formation (AP scaffold), the intensity of absorption peaks of PVA at 849, 1096, 1336, 1440, and 2944 cm^{-1} decreased, and some peaks (such as 1250, 1370 and 1720) disappeared. In other words, the SA characteristic bonds appeared at 1615, 1417, and 3430 cm^{-1} could be observed in the spectra of the blend. FTIR spectrum of electrospun AP scaffold indicated the formation of hydrogen bonding between the hydroxyl group of PVA and alginate which moderated the interaction between alginate macromolecules and amended the electro-spinnability of SA with PVA [26].

FTIR spectra of Gr content scaffolds, before crosslinking process, revealed that there was no chemical interaction between polymer matrices and Gr nanosheets which might be due to the absence of any functional groups on the surface of Gr nanosheets [48]. After crosslinking process, C-C and C-H bonds of Gr incorporated scaffolds, specifically AP-2Gr and AP-5Gr, shifted to lower wave numbers and their intensities reduced. It might be due to the effect of environment (in the crosslinking procedure) on the pristine Gr nanosheets or in the process of preparation of graphene that caused to form functional groups on their surface leading to the physical/chemical interactions between polymeric and graphene.

ACCEPTED MANUSCRIPT

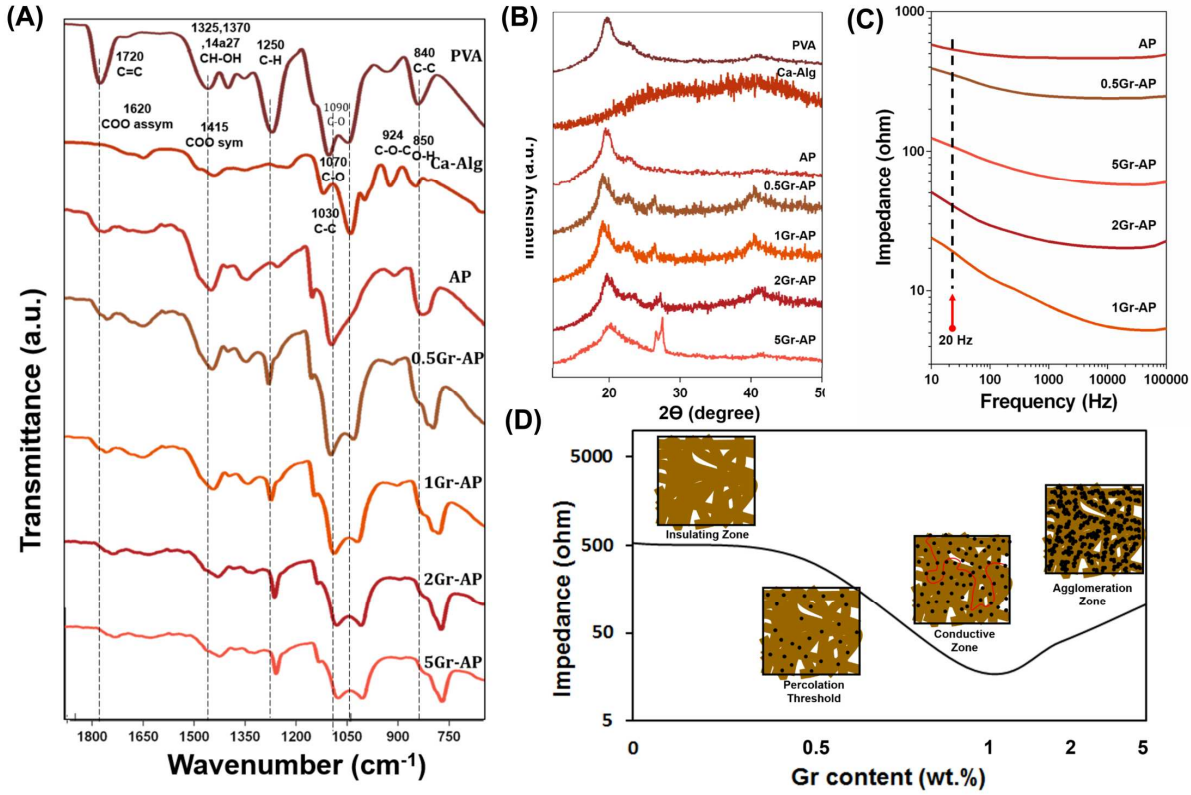

Fig. 3. Chemical and electrical characteristics of Gr-AP scaffolds; A) ATR-FTIR spectra and B) XRD patterns of fibrous scaffolds consisting of various amounts of Gr nanosheets, after crosslinking process. (The FTIR spectra and XRD patterns of crosslinked pure PVA and alginate (Ca-Alg) were inserted as controls). C) The overall impedance of fibrous scaffolds with various Gr content with thickness of 150 µm evaluated in 2 M H_2SO_4 solution. D) The changes of impedance value of various scaffolds consisting of 0-5 wt.% Gr nanosheets at frequency=20 Hz revealed the presence of a crucial point in which the electrical conductivity was the best. The schematic of the percolation theory revealed that the presence of a crucial point between 0.5-2 in which the broad conductive path was formed through the bridging Gr nanosheets (the red line).

XRD patterns confirmed the results FTIR assay (Fig. 3(B) and Supplementary Fig. S3(A)). Before crosslinking process, electrospun PVA scaffold exhibited a crystalline peak at 2θ=19.3° due to the presence of hydrogen bonding [26]. After blending of PVA and SA, all peaks corresponding to both polymers disappeared and one broad peak at around 2θ=19.6° was observed demonstrating the interaction between the SA and PVA and properly blending of them. Moreover, the presence of this broad peak (at 2θ=19.6°) confirmed that the electrospinning process hindered the crystallization of SA/PVA blend which could be due to the hydrogen-

bonding interaction between hydroxyl groups of PVA and the carboxyl or hydroxyl groups of SA leading to the formation of nanofibers with amorphous microstructure [15]. While XRD pattern of uncrosslinked 1Gr-AP scaffolds consisted of only one broad peak closed to that of PVA at 2θ=19.3°, crosslinked Gr-AP scaffold consisted of a new sharp peak at 2θ = 27° which might be due to the formation of new covalent bonds between Gr nanosheets and the SA/PVA blend. The intensity of this peak enhanced with increasing Gr content up to 5 wt.% (5Gr-AP). This result was similarly reported in other Gr content scaffolds such as PVA/rGO [49] and revealed that Gr nanosheets were uniformly dispersed in the AP matrix and the crystalline structure of polymers was slightly increased by the incorporation of Gr component.

After crosslinking process (Fig. 3(B)), the intensity of the diffraction peak at 2θ=19.6° enhanced with increasing Gr content up to 1 wt.% (1Gr-AP scaffold) and then declined demonstrating that improved crystallinity of 1Gr-AP compared to other scaffolds. Gr nanosheets acted as nucleating agents to improve the crystallinity of the composites. However, at high Gr loading level, the nanosheets tended to restack leading to reduction in surface area compared to lower Gr content scaffolds. Based on this result, the further addition of the Gr nanosheets may hinder the regular arrangements of the SA/PVA chains which was similarly reported elsewhere [50].

Representative Raman spectra of the Gr nanosheets and 1Gr-AP scaffold could confirm the Gr nanosheets-AP matrix interaction (Supplementary Fig. S4). The Gr nanosheet spectrum revealed the prominent bands at around 1580 cm^{-1} (G-band), 2680 cm^{-1} (2D-band) and 1340 cm^{-1} (D-band). While G-band was assigned to graphitic carbons with sp^2 hybridization, the D-band was related to the structural defects (disorder-induced modes) in the graphene sample [51]. Moreover, 2D-band was attributed to the overtone (second harmonic) of the D band [52]. In other words, 1Gr-AP scaffold consisted of the characteristics bands of alginate and PVA along with Gr-nanosheet bands. 1Gr-AP scaffolds revealed the characteristic peaks of PVA at 1360 cm^{-1} and 1443 cm^{-1} corresponding to O-H and C-H bending (indicated by arrow). Moreover, the band at 1143 cm^{-1} assisted as a measure of PVA crystallinity[53]. Other bands in the Raman spectrum of 1Gr-AP were related to sodium alginate. According to the previous researches, the Raman spectrum of alginates consisted of several bands related to the various functional groups of alginate [54]. The main bands could be detected at 1098 cm^{-1} (glycosidic ring breathing

mode), 1300 cm^{-1} (carboxylate stretching vibration) and 1413 cm^{-1} (symmetric carboxylate stretching vibration). In addition, the D band of Gr-nanosheets was partially superimposed to the carboxylate stretching vibration band of alginate. Moreover, the intensity of 2D-band of Gr nanosheets was significantly reduced when dispersed in the AP matrix. This behavior was similarly reported in previous research and might be due to the interaction of the Gr nanosheets and AP matrix which demonstrated the well homogeneous dispersion of Gr in the matrix [55].

Impedance analysis (Fig. 3 (C)) demonstrated that all fibrous scaffolds revealed low impedance at physiologically relevant frequencies (20 Hz) [56] due to capacitive currents. Moreover, the impedance of Gr-AP was noticeably lower than that of AP scaffold (Figs. 3(C, D)). Specifically, incorporation of 1 wt.% Gr nanosheets resulted in significantly reduced the impedance of AP scaffold (from 450 ohm to 25 ohm at 20 Hz (Fig. 3(D))), which attributed to the formation of conductive networks by Gr nanosheets. However, according to Figs. 3(C, D), there was a critical concentration of Gr nanosheets to improve electrical conductivity depending on their dispersion or degree of agglomeration. Based on previous studies, in order to coagulate Gr nanosheets to form network which accelerates the electrical conduction in a composite structure, it is critical to provide a balance between Gr nanosheets and Gr nanosheets-matrix interactions [57]. This balance could be gained in a critical concentration of Gr nanosheets called the percolation threshold in which the polymer composites changed from insulating to conducting system [58]. Based on our results, the concentration of Gr nanosheets at percolation threshold point was about 0.5 wt.%. At this point, tunneling effects [59] happened between adjacent Gr nanosheets (Fig. 3(D)) leading to a slight increase in the conductivity. According to the schematic presented in Fig. 3(D), increasing the concentration of Gr nanosheets upon 1 wt.% (1Gr-AP) resulted in the formation of a broad conductive path through the bridging Gr nanosheets (the red lines in the schematic at Fig. 3(D)) at the percolation leading to significantly reduced impedance value. Our result demonstrated that, hybrid 1Gr-AP scaffold, with relatively higher concentration than the percolation threshold of Gr (0.5 wt.%), exhibited lower electrical impedance than other scaffolds (Fig. 3(C)) which might promote electrical signal propagation and coupling distal and proximal of injured nerve tissue [60]. Incorporation of more Gr nanosheets (≥2 wt.%) enhanced the number of conducting networks until the conductivity value reduced (impedance value of 5Gr-AP= 106 ohm) which might be due to the agglomeration and

formation of resistant path in the structure [57]. Recently, similar studies were performed, which demonstrated the crucial role of polymer matric, fabrication process as well as conducting particles on the percolation threshold [58, 61]. For instance, He *et al.* [61] prepared Gr/polyvinylidene fluoride (PVDF) composites using in-situ solvothermal reduction of graphene oxide in the PVDF solution. The percolation threshold of such composite was determined to be 0.31 vol.%, and loading 0.5 vol.% graphene oxide resulted in significantly promoted dielectric constant compared to PVDF matrix. Researches demonstrated the effective role of peripheral nerve stimulation at low-frequency (20 Hz for 1 h) in the successful treatment of medically refractory neuropathic pain [56]. Low-frequency electrical stimulation could accelerate axonal regeneration in patients with median nerve compression in the carpal tunnel affecting the noticeable motor axonal loss. Our findings indicated that 1Gr-AP scaffolds with low impedance at physiologically relevant frequencies might be helpful for improved nerve regeneration during stimulation.

One of the critical properties of neural graft is to provide appropriate mechanical properties in order to support severe physiological loading conditions [4]. The Gr-AP scaffolds revealed robust construct along with significant strain at break (Fig. 4(A)). Tensile test was performed to measure the stiffness, strength, elongation and toughness of the fibrous scaffolds in accordance with common procedures widely applied in engineering mechanical studies of ultrathin films and membrane (ASTM D882). The typical stress–strain curves of hybrid Gr-AP scaffolds after crosslinking treatment and immersing in PBS for 1 h are shown in Fig. 4(B). These trends indicated that the mechanical properties of scaffolds were significantly controlled by Gr nanosheet content. In particular, the incorporation of Gr nanosheets noticeably improved the strength of the scaffold from 7.3±0.5 (AP scaffold) to 22.1 ±2.2 (1Gr-AP scaffold) and 28.8 ±4.3 MPa (5Gr-AP), respectively ($P<0.05$) (Supplementary Fig S5(A)). In other words, compared to AP scaffold, the toughness of 1Gr-AP and 2Gr-AP scaffolds considerably improved (4 and 5.5-fold, respectively) from 2.1±1.2 MPa to 8.1±3.5 MPa and 11.0±2.6 MPa, respectively (Supplementary Fig. S5(B)). However, the incorporation of Gr nanosheets more than 2 wt.% resulted in a noticeably reduction of the elongation (48.1±12.2 %) even lower than that of pure AP scaffold (72.4±18.2 %) (Supplementary Fig. S5(D)), while tensile modulus prominently enhanced (7-folds) (Supplementary Fig. S5(C)). Similar results was reported for alginate-

graphene oxide fibrous scaffolds prepared by wet spinning when GO content was about 4 wt.% [62]. It might be due to the aggregation of the incorporated Gr nanosheets which resulted in the formation of micron-sized agglomerates in Gr-AP constructs (Fig. 4(C)).

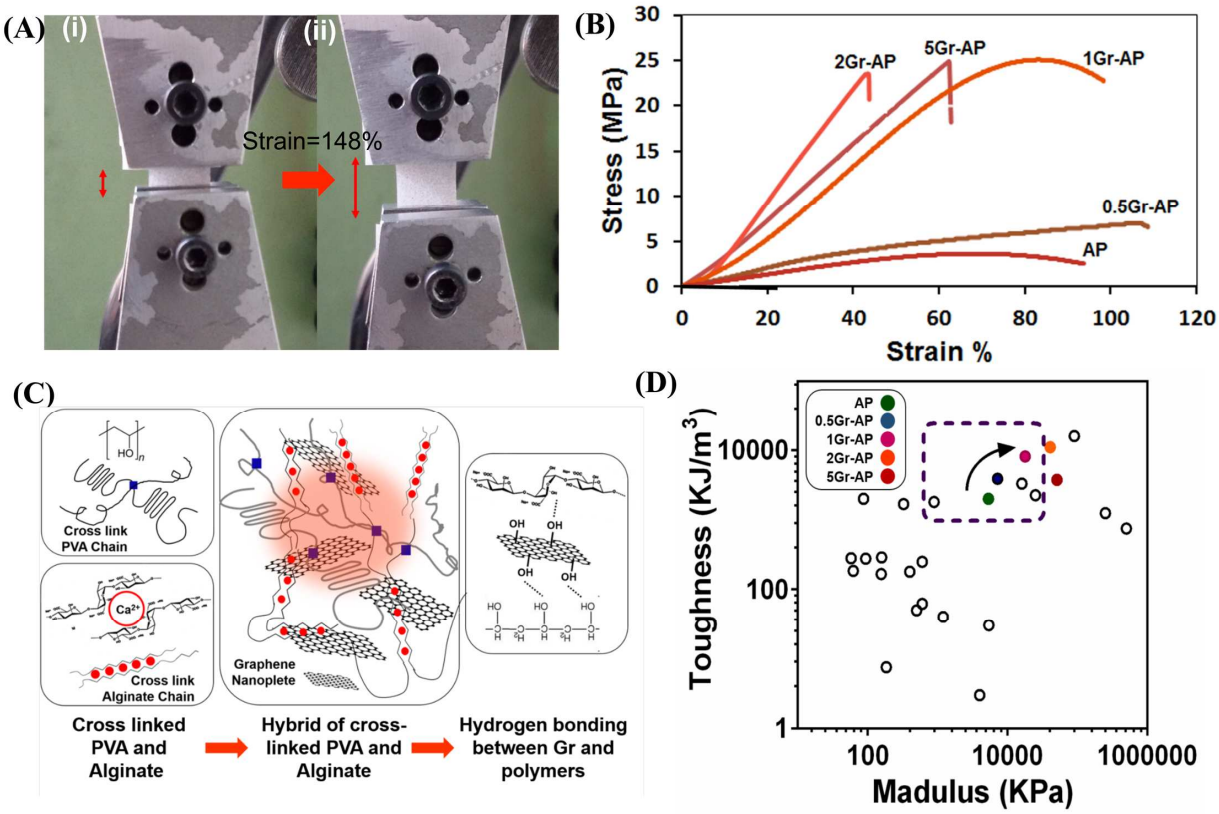

Fig. 4. Mechanical properties of fibrous samples consisting of various amounts of Gr nanosheets; A) The representative image of 1Gr-AP scaffold (i) before and (ii) during the tensile loading. Hybrid 1Gr-AP fibrous scaffold exhibited resistance to fracture at high strain during uniaxial tensile test (148%). B) Representative uniaxial tensile stress-strain plots of crosslinked nanofibrous scaffolds after 1 days soaking in PBS. C) Schematic illustrating the formation of the interpenetrating network of PVA:SA, via physical crosslinking of PVA by heat treatment and chemical crosslinking of Alginate by CaCl2 solution, as well as the hydrogen bonding between Gr nanosheets and polymer matrix leading to significantly promoted mechanical properties. D) Comparison of the elastic moduli and toughness for previously reported compliant fibrous scaffolds (open circle) [41, 63-69] and the proposed Gr-AP scaffolds in hydrated state. The dashed window demonstrates the area with the best mechanical properties for nerve tissue engineering. Black arrow revealed that the toughness of AP fibrous scaffolds noticeably promoted via incorporation of 1 wt.% Gr nanosheets

Based on our results, hybrid 1Gr-AP fibrous scaffold revealed superior mechanical properties

than others, due to simultaneously enhancement of tensile strength, toughness and elongation while tensile modulus did not significantly change. It could be attributed to the formation of semi-IPN with superior mechanical properties than pure PVA and SA, uniform dispersion of Gr nanosheets in the AP matrix as well as the interphase reinforcement mechanism which is based on the formation of extended interphase zones between two components in hybrid constructs [22, 26]. It is worth noting that, in the case of Gr nanosheets, the interphase region might play a significant role, since the filler was below 5 nm thick [70]. These factors were schematically illustrated in Fig. 4(C). As depicted in Fig. 4(C) and demonstrated in Fig. 3(A), after crosslinking process, the oxygen containing groups of Gr nanosheets could chemically interact with hydroxyl or carbonyl groups of AP matrix leading to effectively transfer the mechanical loads from the matrix to Gr nanosheets and improved tensile strength. Moreover, the highly flexible sheet structure of Gr could efficiently dissipate energy applied to the polymer matrix through highly dynamic conformational changes, and therefore had a profound influence on the hydrogel toughness. Therefore, the incorporation of 1 wt.% Gr nanosheets into polymer matrix could be highly useful to improve the mechanical strength, elongation and specially toughness without significantly affect on the rigidity which could be beneficial for soft tissue engineering such as nerve and cardiac [49, 70]. Incorporation of more Gr nanosheets (≥2 wt.%) within the scaffolds resulted in their agglomeration leading to reduce in toughness and elongation which may not appropriate for nerve tissue engineering.

Based on wide researches, the mechanical properties of a cell's environment affect the broad range of its properties, ranging from the morphology of cells and tissues, to cell motility directed by substrate stiffness [45]. Latest results suggested that the cells of peripheral nervous system displayed alterable neurite extension and branching depending on the mechanical properties, such as tensile modulus and toughness, of substrates [71]. Specifically, the toughness is one of the crucial properties of neural engineering scaffolds allowing it to recover once the construct is employed around the nerve [72], to manipulate easily, to bear shocks and vibrations, to cut into strips or other shapes and to be rolled up into 3D tubular construct [73, 74]. Our results demonstrated that 1Gr-AP scaffold revealed the superior toughness as compared to previously reported scaffolds which made it suitable for nerve tissue engineering (Fig. 4(D)) [38, 41, 64, 66, 67, 69, 75-78]. For instance, while the toughness of 1Gr-AP scaffolds were about 8.1±3.5 MPa,

PCL/gelatin fibrous scaffold showed the toughness of about 1.13 MPa [79]. Furthermore, our results revealed that, the toughness, elastic modulus and strength of 1Gr-AP were 5.37±1.8 MPa and 23.7±12.3 MPa and 20.16±1.8 MPa, respectably, which were the nearest mechanical properties to those of the native nerve trunk [80, 81]. Our data demonstrated that hybrid 1Gr-AP scaffold which is not only electrically conductive but also mechanically mimic the native tissue could be a promising new candidate for engineering nerve tissue.

3.2 Cell morphology and proliferation

The cell morphology is an important factor in determining the biocompatibility of a biomaterial. As fibrous scaffolds morphologically mimic the ECM structure of native tissues, they offer a promising matrix for the cell attachment and proliferation. SEM images of PC12 cells cultured for 1 and 7 days on the various scaffolds are presented in Figs. 5 and 6, respectively. After a day of culture (Fig. 5), cells adhered tightly to the scaffolds with rounded morphology and formed colonies in good agreement with previously published studies [82]. The arrows in the figures pointed to the cell colonies formed on various scaffolds after one day of culture. However, the number of attached cells varied depending on the scaffold type. Fig. 5(F) revealed a significant modulation in the cell retention (fraction of scaffold surface covered with cells) as a function of Gr concentration. The cell retention drastically enhanced from 0.12±0.02% (for AP scaffold) to 0.18 ±0.01% (for 1Gr-AP scaffold)which might be due to the electrical conductance of Gr-AP scaffolds and significantly improved mechanical properties. After 7 days of culture, the morphology of cells changed according to the scaffold type. While cells seeded on the AP fibrous scaffold preserved a rounded morphology with little spreading, polygonal appearance of PC12 cells could be observed on hybrid 1Gr-AP scaffold which connected with the neighboring cells, implying their preparedness and initiation to differentiate [83]. Moreover, according to the estimated average cell area after 7 days of culture (Fig. 6(F)), PC12 cells covered more surface area of the scaffolds than that of after 1 days of culture. For instance, at 1Gr-AP scaffold, after 7 days of culture, cell area was 2.1-fold greater than that of after 1 day of culture. Additionally, the average cell area covered 1Gr-AP scaffold, after 7 days of culture (0.40±0.01), was significantly enhanced by 2.9 times compared to that of on AP scaffold (0.14±0.02). Furthermore, the incorporation of more Gr content upon 1 wt.% resulted in reduced cell area, which might be due to the enhanced hydrophobic nature as well as less electrical

conductivity of fibrous scaffolds.

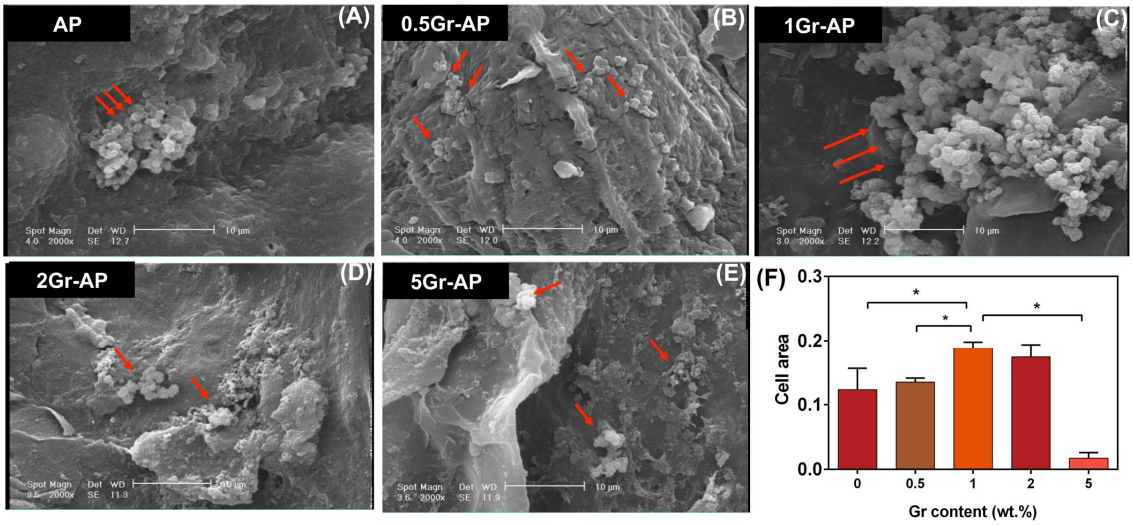

Fig. 5. PC12 cell attachment on the various fibrous scaffolds; SEM images of PC12 cells after 1 day of culture on A) AP, B) 0.5Gr-AP, C) 1Gr-AP, D) 2Gr-AP and E) 5Gr-AP fibrous scaffolds. Red arrows show the formation of cell colony and its distribution. E) Cell retention, the fraction of area covered with cell clusters, on the fibrous scaffolds as a function of Gr content (* $P < 0.05$).

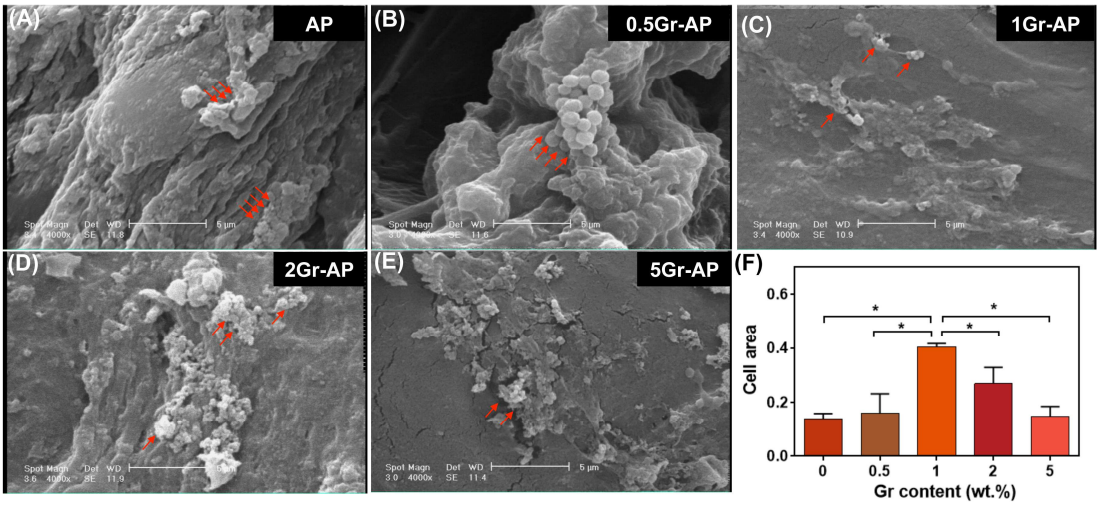

Fig. 6. PC12 cell spreading on the various fibrous scaffolds; SEM images of PC12 cells after 7 days of culture on A) AP, B) 0.5Gr-AP, C) 1Gr-AP, D) 2Gr-AP and E) 5Gr-AP fibrous scaffolds. Red arrows show the distribution and spreading of PC12 cells. E) Cell spreading, the fraction of area covered with cell clusters, on the fibrous scaffolds as a function of Gr content (* $P < 0.05$).

MTT assay was performed to evaluate the metabolic activity of the proliferating cells seeded on the scaffolds. The MTT assay (Fig. 7) demonstrated that the proliferation of PC12 cells gradually enhanced on hybrid scaffolds from day 1 to day 7. Specifically, the proliferation of cells cultured on the 1Gr-AP scaffold statistically enhanced from 113.2±2.12 (% control) (at day 1) to 244.4 ±10.3 (%control) (at day 7) ($P<0.05$). Moreover, the number of metabolically active cells grown on the Gr embedded scaffolds was significantly higher than that of on the AP scaffold ($P<0.05$). For instance, after 7 days of culture, the proliferation of cells cultured on the 0.5Gr-AP, 2Gr-AP and 5Gr-AP scaffolds was improved by 1.04, 1.31, 0.75 and 0.95 times, respectively, compared to AP scaffold. These results confirmed the effects of mechanical and electrical properties on the proliferation of cells. In a similar report, Gopinathan *et al.* [84] suggested that the inclusion of nano-fillers, particularly carbon-nanofiber could improve the cytocompatibility and proliferation of PC12 cell compared to PCL scaffold. However, at high Gr embedded AP scaffold (2-5 wt. %), cell proliferation decreased compared to that of 1Gr-AP scaffold (1.1 and 1.2 times of 1Gr-AP, respectively). Our results revealed that despite the important role of Gr nanosheets in the bioactivity of polymeric biomaterials [85], the inhibitory effect on PC12 cell proliferation at high Gr concentration could be observed which might be due to the release of Gr nanosheets in the environment.

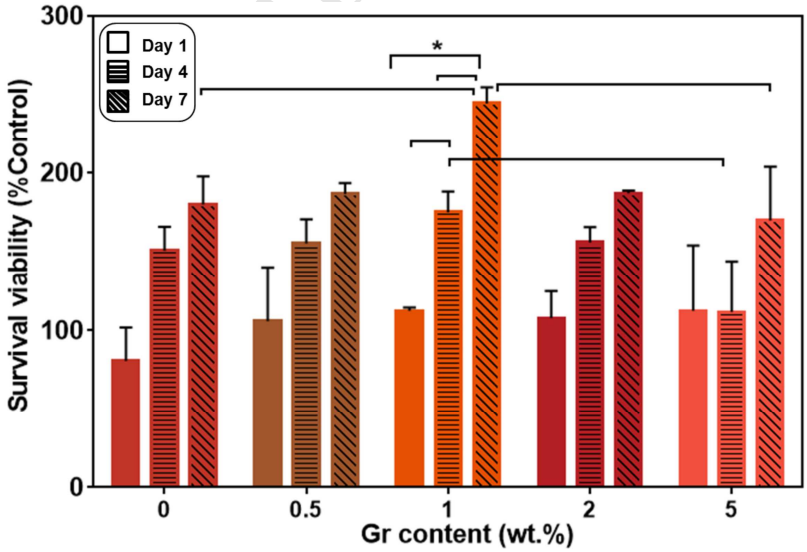

Fig. 7. Cell viability of PC12 on various fibrous scaffolds measured using MTT assays after 1, 3 and 7 days of culture. The absorbance was normalized against the control (TCP) at each time interval. (*$P < 0.05$).

Our findings obviously proved that Gr incorporated AP scaffold presented higher PC12 cell adhesion moieties, thereby promoting cell retention, specifically at the initial points of culture. Between the samples, PC12 cells could well spread on the surface of 1Gr-AP which might be due to the superior electrical and mechanical properties than other scaffolds. However, according to previous studies, the incorporation of carbon based nanomaterials into natural substrates revealed enhanced cellular adhesion and proliferation due to the forceful attraction between the nanomaterials and the polymers [86]. In conclusion, engineering substrates to induce preferred cell behavior is a principal strategy of scaffold design for tissue-engineering applications. We demonstrated that hybrid Gr-AP fibrous scaffold could highly promoted PC12 cell adhesion, spreading, and proliferation.

Conclusion

In summary, hybrid fibrous scaffolds composed of sodium alginate, PVA and Gr nanosheets were successfully developed using electrospinning technique. Non-covalent bonding between Gr nanosheets and PVA:alginate matrix provided homogenous dispersion of Gr nanosheets in the alginate: PVA hybrid matrices leading to considerable improvement of electrical and mechanical properties. Notably, the incorporation of 1 wt.% Gr nanosheets enhanced the toughness and strength of the scaffolds by 4- and 3-fold while tensile modulus did not significantly modulate. Moreover, addition of Gr nanosheet upon 1 wt.% resulted in a significant reduction in impedance value (18-fold) a due to the formation of broad conductive path through the bridging Gr nanosheets. In addition, the Gr-AP matrices can effectively enhance the initial attachment, spreading and proliferation of PC12 cells according to superior electrical and mechanical properties. These results recommended that this hybrid 1Gr-AP fibrous scaffold with superior electrical conductivity, strength and toughness provide a suitable matrix to support cellular responses in comparison to previously reported Gr -incorporated scaffolds for nerve tissue engineering. In our future work, we aim to stack these fibrous layers in order to develop a complex and thick nerve conduit.

Reference

[1] J. Isaacs, Major peripheral nerve injuries, Hand clinics 29(3) (2013) 371-82.

[2] R. Deumens, A. Bozkurt, M.F. Meek, M.A. Marcus, E.A. Joosten, J. Weis, G.A. Brook, Repairing injured peripheral nerves: bridging the gap, Progress in neurobiology 92(3) (2010) 245-276.
[3] S. Panseri, C. Cunha, J. Lowery, U. Del Carro, F. Taraballi, S. Amadio, A. Vescovi, F. Gelain, Electrospun micro- and nanofiber tubes for functional nervous regeneration in sciatic nerve transections, BMC biotechnology 8 (2008) 39.
[4] A.R. Nectow, K.G. Marra, D.L. Kaplan, Biomaterials for the development of peripheral nerve guidance conduits, Tissue engineering. Part B, Reviews 18(1) (2012) 40-50.
[5] G.C. de Ruiter, M.J. Malessy, M.J. Yaszemski, A.J. Windebank, R.J. Spinner, Designing ideal conduits for peripheral nerve repair, Neurosurgical focus 26(2) (2009) E5.
[6] S. Yang, K.-F. Leong, Z. Du, C.-K. Chua, The design of scaffolds for use in tissue engineering. Part I. Traditional factors, Tissue engineering 7(6) (2001) 679-689.
[7] D. Gupta, J. Venugopal, M.P. Prabhakaran, V.R. Dev, S. Low, A.T. Choon, S. Ramakrishna, Aligned and random nanofibrous substrate for the in vitro culture of Schwann cells for neural tissue engineering, Acta biomaterialia 5(7) (2009) 2560-9.
[8] T. Hashimoto, Y. Suzuki, K. Suzuki, T. Nakashima, M. Tanihara, C. Ide, Review Peripheral nerve regeneration using non-tubular alginate gel crosslinked with covalent bonds, Journal of Materials Science: Materials in Medicine 16(6) (2005) 503-509.
[9] V. Jayawarna, M. Ali, T.A. Jowitt, A.F. Miller, A. Saiani, J.E. Gough, R.V. Ulijn, Nanostructured Hydrogels for Three-Dimensional Cell Culture Through Self-Assembly of Fluorenylmethoxycarbonyl–Dipeptides, Advanced Materials 18(5) (2006) 611-614.
[10] E. Alsberg, E. Feinstein, M. Joy, M. Prentiss, D.E. Ingber, Magnetically-guided self-assembly of fibrin matrices with ordered nano-scale structure for tissue engineering, Tissue engineering 12(11) (2006) 3247-3256.
[11] S. Tang, J. Zhu, Y. Xu, A.P. Xiang, M.H. Jiang, D. Quan, The effects of gradients of nerve growth factor immobilized PCLA scaffolds on neurite outgrowth in vitro and peripheral nerve regeneration in rats, Biomaterials 34(29) (2013) 7086-7096.
[12] J. Xie, M.R. MacEwan, W. Liu, N. Jesuraj, X. Li, D. Hunter, Y. Xia, Nerve guidance conduits based on double-layered scaffolds of electrospun nanofibers for repairing the peripheral nervous system, ACS applied materials & interfaces 6(12) (2014) 9472-80.
[13] T.J. Sill, H.A. von Recum, Electrospinning: applications in drug delivery and tissue engineering, Biomaterials 29(13) (2008) 1989-2006.
[14] P. Prang, R. Muller, A. Eljaouhari, K. Heckmann, W. Kunz, T. Weber, C. Faber, M. Vroemen, U. Bogdahn, N. Weidner, The promotion of oriented axonal regrowth in the injured spinal cord by alginate-based anisotropic capillary hydrogels, Biomaterials 27(19) (2006) 3560-9.
[15] K.T. Shalumon, K.H. Anulekha, S.V. Nair, S.V. Nair, K.P. Chennazhi, R. Jayakumar, Sodium alginate/poly(vinyl alcohol)/nano ZnO composite nanofibers for antibacterial wound dressings, International journal of biological macromolecules 49(3) (2011) 247-54.
[16] M.S. Kim, G. Kim, Three-dimensional electrospun polycaprolactone (PCL)/alginate hybrid composite scaffolds, Carbohydrate polymers 114 (2014) 213-21.
[17] H. Hajiali, J.A. Heredia-Guerrero, I. Liakos, A. Athanassiou, E. Mele, Alginate nanofibrous mats with adjustable degradation rate for regenerative medicine, Biomacromolecules 16(3) (2015) 936-43.
[18] H. Omidian, J.G. Rocca, K. Park, Elastic, superporous hydrogel hybrids of polyacrylamide and sodium alginate, Macromolecular bioscience 6(9) (2006) 703-10.
[19] W. Shen, Y.L. Hsieh, Biocompatible sodium alginate fibers by aqueous processing and physical crosslinking, Carbohydrate polymers 102 (2014) 893-900.
[20] N. Royo-Gascon, M. Wininger, J.I. Scheinbeim, B.L. Firestein, W. Craelius, Piezoelectric substrates promote neurite growth in rat spinal cord neurons, Annals of biomedical engineering 41(1) (2013) 112-22.

[21] S. Naghavi Alhosseini, F. Moztarzadeh, S. Kargozar, M. Dodel, M. Tahriri, Development of Polyvinyl Alcohol Fibrous Biodegradable Scaffolds for Nerve Tissue Engineering Applications:In VitroStudy, International Journal of Polymeric Materials and Polymeric Biomaterials 64(9) (2015) 474-480.
[22] F.G. Thankam, J. Muthu, V. Sankar, R.K. Gopal, Growth and survival of cells in biosynthetic poly vinyl alcohol–alginate IPN hydrogels for cardiac applications, Colloids and Surfaces B: Biointerfaces 107 (2013) 137-145.
[23] M.P. Prabhakaran, L. GhasemiMobarakeh, G. Jin, S. Ramakrishna, Electrospun conducting polymer nanofibers and electrical stimulation of nerve stem cells, Journal of bioscience and bioengineering 112(5) (2011) 501-7.
[24] S. Naficy, S. Kawakami, S. Sadegholvaad, M. Wakisaka, G.M. Spinks, Mechanical properties of interpenetrating polymer network hydrogels based on hybrid ionically and covalently crosslinked networks, Journal of Applied Polymer Science 130(4) (2013) 2504-2513.
[25] M. Shivashankar, B.K. Mandal, A review on interpenetrating polymer network, International Journal of Pharmacy and Pharmaceutical Sciences 4(Suppl 5) (2012).
[26] M.S. Islam, M.R. Karim, Fabrication and characterization of poly(vinyl alcohol)/alginate blend nanofibers by electrospinning method, Colloids and Surfaces A: Physicochemical and Engineering Aspects 366(1-3) (2010) 135-140.
[27] G. Shi, M. Rouabhia, Z. Wang, L.H. Dao, Z. Zhang, A novel electrically conductive and biodegradable composite made of polypyrrole nanoparticles and polylactide, Biomaterials 25(13) (2004) 2477-2488.
[28] T. Ding, W.W. Lu, Y. Zheng, Z.Y. Li, H.B. Pan, Z. Luo, Rapid repair of rat sciatic nerve injury using a nanosilver-embedded collagen scaffold coated with laminin and fibronectin, Regenerative medicine 6(4) (2011) 437-447.
[29] Y.-L. Lin, J.-C. Jen, S.-h. Hsu, M. Chiu, Sciatic nerve repair by microgrooved nerve conduits made of chitosan-gold nanocomposites, Surgical neurology 70 (2008) S9-S18.
[30] F. Mottaghitalab, M. Farokhi, A. Zaminy, M. Kokabi, M. Soleimani, F. Mirahmadi, M.A. Shokrgozar, M. Sadeghizadeh, A biosynthetic nerve guide conduit based on silk/SWNT/fibronectin nanocomposite for peripheral nerve regeneration, (2013).
[31] M. Tang, Q. Song, N. Li, Z. Jiang, R. Huang, G. Cheng, Enhancement of electrical signaling in neural networks on graphene films, Biomaterials 34(27) (2013) 6402-11.
[32] J. Huang, H. Deng, D. Song, H. Xu, Electrospun polystyrene/graphene nanofiber film as a novel adsorbent of thin film microextraction for extraction of aldehydes in human exhaled breath condensates, Analytica chimica acta 878 (2015) 102-8.
[33] N. Li, Q. Zhang, S. Gao, Q. Song, R. Huang, L. Wang, L. Liu, J. Dai, M. Tang, G. Cheng, Three-dimensional graphene foam as a biocompatible and conductive scaffold for neural stem cells, Scientific reports 3 (2013) 1604.
[34] C. Li, T. Hou, X. She, X. Wei, F. She, W. Gao, L. Kong, Decomposition properties of PVA/graphene composites during melting-crystallization, Polymer Degradation and Stability 119 (2015) 178-189.
[35] T. Zhou, F. Chen, C. Tang, H. Bai, Q. Zhang, H. Deng, Q. Fu, The preparation of high performance and conductive poly (vinyl alcohol)/graphene nanocomposite via reducing graphite oxide with sodium hydrosulfite, Composites Science and Technology 71(9) (2011) 1266-1270.
[36] N. Thayumanavan, P. Tambe, G. Joshi, M. Shukla, Effect of sodium alginate modification of graphene (by 'anion-π' type of interaction) on the mechanical and thermal properties of polyvinyl alcohol (PVA) nanocomposites, Composite Interfaces 21(6) (2014) 487-506.
[37] J.T. Rutka, G. Apodaca, R. Stern, M. Rosenblum, The extracellular matrix of the central and peripheral nervous systems: structure and function, Journal of neurosurgery 69(2) (1988) 155-170.
[38] Y. Qi, Z. Tai, D. Sun, J. Chen, H. Ma, X. Yan, B. Liu, Q. Xue, Fabrication and characterization of poly (vinyl alcohol)/graphene oxide nanofibrous biocomposite scaffolds, Journal of Applied Polymer Science 127(3) (2013) 1885-1894.

[39] K.Y. Lee, L. Jeong, Y.O. Kang, S.J. Lee, W.H. Park, Electrospinning of polysaccharides for regenerative medicine, Advanced Drug Delivery Reviews 61(12) (2009) 1020-1032.
[40] N. Bhattarai, D. Edmondson, O. Veiseh, F.A. Matsen, M. Zhang, Electrospun chitosan-based nanofibers and their cellular compatibility, Biomaterials 26(31) (2005) 6176-84.
[41] M. Kharaziha, S.R. Shin, M. Nikkhah, S.N. Topkaya, N. Masoumi, N. Annabi, M.R. Dokmeci, A. Khademhosseini, Tough and flexible CNT-polymeric hybrid scaffolds for engineering cardiac constructs, Biomaterials 35(26) (2014) 7346-54.
[42] A. Oskouyi, U. Sundararaj, P. Mertiny, Tunneling Conductivity and Piezoresistivity of Composites Containing Randomly Dispersed Conductive Nano-Platelets, Materials 7(4) (2014) 2501-2521.
[43] T.N. Zhou, The preparation of the poly(vinyl alcohol)/graphene nanocomposites with low percolation threshold and high electrical conductivity by using the large-area reduced graphene oxide sheets, Express Polymer Letters 7(9) (2013) 747-755.
[44] J. Wang, X. Wang, C. Xu, M. Zhang, X. Shang, Preparation of graphene/poly (vinyl alcohol) nanocomposites with enhanced mechanical properties and water resistance, Polymer International 60(5) (2011) 816-822.
[45] C. Cha, S.R. Shin, X. Gao, N. Annabi, M.R. Dokmeci, X.S. Tang, A. Khademhosseini, Controlling mechanical properties of cell-laden hydrogels by covalent incorporation of graphene oxide, Small 10(3) (2014) 514-23.
[46] Y.-T. Jia, J. Gong, X.-H. Gu, H.-Y. Kim, J. Dong, X.-Y. Shen, Fabrication and characterization of poly (vinyl alcohol)/chitosan blend nanofibers produced by electrospinning method, Carbohydrate polymers 67(3) (2007) 403-409.
[47] J.M. Gohil, A. Bhattacharya, P. Ray, Studies On The Crosslinking Of Poly (Vinyl Alcohol), Journal of Polymer Research 13(2) (2005) 161-169.
[48] S. Radic, N.K. Geitner, R. Podila, A. Käkinen, P. Chen, P.C. Ke, F. Ding, Competitive binding of natural amphiphiles with graphene derivatives, Scientific reports 3 (2013).
[49] Y. Xu, W. Hong, H. Bai, C. Li, G. Shi, Strong and ductile poly (vinyl alcohol)/graphene oxide composite films with a layered structure, Carbon 47(15) (2009) 3538-3543.
[50] X. Zhao, Q. Zhang, D. Chen, P. Lu, Enhanced mechanical properties of graphene-based poly (vinyl alcohol) composites, Macromolecules 43(5) (2010) 2357-2363.
[51] A.C. Ferrari, Raman spectroscopy of graphene and graphite: disorder, electron–phonon coupling, doping and nonadiabatic effects, Solid state communications 143(1) (2007) 47-57.
[52] X. Zhao, Q. Zhang, D. Chen, P. Lu, Enhanced Mechanical Properties of Graphene-Based Poly(vinyl alcohol) Composites, Macromolecules 44(7) (2011) 2392-2392.
[53] C. Wang, Y. Li, G. Ding, X. Xie, M. Jiang, Preparation and characterization of graphene oxide/poly (vinyl alcohol) composite nanofibers via electrospinning, Journal of Applied Polymer Science 127(4) (2013) 3026-3032.
[54] T. Schmid, A. Messmer, B.-S. Yeo, W. Zhang, R. Zenobi, Towards chemical analysis of nanostructures in biofilms II: tip-enhanced Raman spectroscopy of alginates, Analytical and bioanalytical chemistry 391(5) (2008) 1907-1916.
[55] F. Barzegar, A. Bello, M. Fabiane, S. Khamlich, D. Momodu, F. Taghizadeh, J. Dangbegnon, N. Manyala, Preparation and characterization of poly (vinyl alcohol)/graphene nanofibers synthesized by electrospinning, Journal of Physics and Chemistry of Solids 77 (2015) 139-145.
[56] B.J. Pfister, T. Gordon, J.R. Loverde, A.S. Kochar, S.E. Mackinnon, D.K. Cullen, Biomedical engineering strategies for peripheral nerve repair: surgical applications, state of the art, and future challenges, Critical Reviews™ in Biomedical Engineering 39(2) (2011).
[57] P.N. Khanam, D. Ponnamma, M. AL-Madeed, Electrical Properties of Graphene Polymer Nanocomposites, Graphene-Based Polymer Nanocomposites in Electronics, Springer2015, pp. 25-47.

[58] Y. Wang, J.W. Shan, G.J. Weng, Percolation threshold and electrical conductivity of graphene-based nanocomposites with filler agglomeration and interfacial tunneling, Journal of Applied Physics 118(6) (2015) 065101.
[59] W.S. Bao, S.A. Meguid, Z.H. Zhu, G.J. Weng, Tunneling resistance and its effect on the electrical conductivity of carbon nanotube nanocomposites, Journal of Applied Physics 111(9) (2012) 093726.
[60] <583.pdf>.
[61] L. He, S.C. Tjong, Low percolation threshold of graphene/polymer composites prepared by solvothermal reduction of graphene oxide in the polymer solution, Nanoscale research letters 8(1) (2013) 132.
[62] Y. He, N. Zhang, Q. Gong, H. Qiu, W. Wang, Y. Liu, J. Gao, Alginate/graphene oxide fibers with enhanced mechanical strength prepared by wet spinning, Carbohydrate polymers 88(3) (2012) 1100-1108.
[63] W. Daamen, Preparation and evaluation of molecularly-defined collagen–elastin–glycosaminoglycan scaffolds for tissue engineering, Biomaterials 24(22) (2003) 4001-4009.
[64] M.C. McManus, E.D. Boland, H.P. Koo, C.P. Barnes, K.J. Pawlowski, G.E. Wnek, D.G. Simpson, G.L. Bowlin, Mechanical properties of electrospun fibrinogen structures, Acta biomaterialia 2(1) (2006) 19-28.
[65] M.L. Minus, H.G. Chae, S. Kumar, Interfacial Crystallization in Gel-Spun Poly(vinyl alcohol)/Single-Wall Carbon Nanotube Composite Fibers, Macromolecular Chemistry and Physics 210(21) (2009) 1799-1808.
[66] S. Zhang, Y. Huang, X. Yang, F. Mei, Q. Ma, G. Chen, S. Ryu, X. Deng, Gelatin nanofibrous membrane fabricated by electrospinning of aqueous gelatin solution for guided tissue regeneration, Journal of biomedical materials research. Part A 90(3) (2009) 671-9.
[67] D. Kai, M.P. Prabhakaran, G. Jin, S. Ramakrishna, Guided orientation of cardiomyocytes on electrospun aligned nanofibers for cardiac tissue engineering, Journal of biomedical materials research. Part B, Applied biomaterials 98(2) (2011) 379-86.
[68] H. Liao, R. Qi, M. Shen, X. Cao, R. Guo, Y. Zhang, X. Shi, Improved cellular response on multiwalled carbon nanotube-incorporated electrospun polyvinyl alcohol/chitosan nanofibrous scaffolds, Colloids and surfaces. B, Biointerfaces 84(2) (2011) 528-35.
[69] M.P. Prabhakaran, D. Kai, L. Ghasemi-Mobarakeh, S. Ramakrishna, Electrospun biocomposite nanofibrous patch for cardiac tissue engineering, Biomedical materials 6(5) (2011) 055001.
[70] K. Hu, M.K. Gupta, D.D. Kulkarni, V.V. Tsukruk, Ultra-robust graphene oxide-silk fibroin nanocomposite membranes, Adv Mater 25(16) (2013) 2301-7.
[71] J.B. Leach, X.Q. Brown, J.G. Jacot, P.A. DiMilla, J.Y. Wong, Neurite outgrowth and branching of PC12 cells on very soft substrates sharply decreases below a threshold of substrate rigidity, Journal of neural engineering 4(2) (2007) 26.
[72] L. Tian, M.P. Prabhakaran, S. Ramakrishna, Strategies for regeneration of components of nervous system: scaffolds, cells and biomolecules, Regenerative Biomaterials 2(1) (2015) 31-45.
[73] G.E. Davis, E. Engvall, S. Varon, M. Manthorpe, Human amnion membrane as a substratum for cultured peripheral and central nervous system neurons, Developmental Brain Research 33(1) (1987) 1-10.
[74] D. Yucel, G.T. Kose, V. Hasirci, Polyester based nerve guidance conduit design, Biomaterials 31(7) (2010) 1596-603.
[75] M. Kharaziha, A. Memic, M. Akbari, D.A. Brafman, M. Nikkhah, Nano-Enabled Approaches for Stem Cell-Based Cardiac Tissue Engineering, Advanced healthcare materials (2016).
[76] Y.C. Shin, J.H. Lee, L. Jin, M.J. Kim, Y.J. Kim, J.K. Hyun, T.G. Jung, S.W. Hong, D.W. Han, Stimulated myoblast differentiation on graphene oxide-impregnated PLGA-collagen hybrid fibre matrices, Journal of nanobiotechnology 13 (2015) 21.

[77] W. Xiangmei, Z. Jing, C. Hao, W. Qingrui, Preparation and characterization of collagen-based composite conduit for peripheral nerve regeneration, Journal of Applied Polymer Science 112(6) (2009) 3652-3662.
[78] D. Cai, K. Yusoh, M. Song, The mechanical properties and morphology of a graphite oxide nanoplatelet/polyurethane composite, Nanotechnology 20(8) (2009) 085712.
[79] L. Ghasemi-Mobarakeh, M.P. Prabhakaran, M. Morshed, M.H. Nasr-Esfahani, S. Ramakrishna, Electrospun poly(epsilon-caprolactone)/gelatin nanofibrous scaffolds for nerve tissue engineering, Biomaterials 29(34) (2008) 4532-9.
[80] G.H. Borschel, K.F. Kia, W.M. Kuzon, R.G. Dennis, Mechanical properties of acellular peripheral nerve, Journal of Surgical Research 114(2) (2003) 133-139.
[81] A.K. Ommaya, Mechanical properties of tissues of the nervous system, Journal of Biomechanics 1(2) (1968) 127-138.
[82] E. Hoveizi, S. Tavakol, S. Ebrahimi-Barough, Neuroprotective effect of transplanted neural precursors embedded on PLA/CS scaffold in an animal model of multiple sclerosis, Molecular neurobiology 51(3) (2015) 1334-1342.
[83] Q. Tian, L. Zhang, J. Liu, N. Li, Q. Ma, J. Zhou, Y. Sun, Coaxial electrospun poly(lactic acid)/silk fibroin nanofibers incorporated with nerve growth factor support the differentiation of neuronal stem cells, RSC Adv. 12 13.
[84] J. Gopinathan, A.F. Quigley, A. Bhattacharyya, R. Padhye, R.M. Kapsa, R. Nayak, R.A. Shanks, S. Houshyar, Preparation, characterisation, and in vitro evaluation of electrically conducting poly(varepsilon-caprolactone)-based nanocomposite scaffolds using PC12 cells, Journal of biomedical materials research. Part A 104(4) (2016) 853-65.
[85] H. Pang, T. Chen, G. Zhang, B. Zeng, Z.-M. Li, An electrically conducting polymer/graphene composite with a very low percolation threshold, Materials Letters 64(20) (2010) 2226-2229.
[86] S. Ahadian, R. Obregón, J. Ramón-Azcón, G. Salazar, H. Shiku, M. Ramalingam, T. Matsue, Carbon Nanotubes and Graphene-Based Nanomaterials for Stem Cell Differentiation and Tissue Regeneration, Journal of Nanoscience and Nanotechnology 16(9) (2016) 8862-8880.

Figure captions:

Fig. 1. A) TEM image of Gr nanosheet. B) Optical images of AP solutions with various concentrations of Gr nanosheets (0, 0.5, 1, 2 and 5 wt.%). C) Schematic diagram describing the fabrication of Gr-AP fibrous scaffold consisting of two steps: preparation of precursor solution (step 1), fabrication and crosslinking of the scaffolds (step 2). Crosslinking process consisted of two steps in which PVA and alginate were crosslinked, consequently.

Fig. 2. Structural and chemical properties of hybrid scaffolds; SEM images of (A, C) AP and (B, D) 1Gr-AP fibrous scaffold, before (A and B) and after (C, D) crosslinking. E) TEM image of 1Gr-AP scaffolds. Magnified image shows the well distribution of Gr nanosheets within the fibrous structure. F) Incorporation of Gr nanosheets significantly changed the average fiber size

of scaffolds, before and after crosslinking process. G) Incorporation of Gr nanosheets also enhanced the water contact angle and, hence, hydrophobicity of scaffolds. H) The changes of degradation rate also revealed the crucial role of Gr nanosheet content on the degradation rate of scaffolds. (* $P < 0.05$).

Fig. 3. Chemical and electrical characteristics of Gr-AP scaffolds; A) ATR-FTIR spectra and B) XRD patterns of fibrous scaffolds consisting of various amounts of Gr nanosheets, after crosslinking process. C) The overall impedance of fibrous scaffolds with various Gr content with thickness of 150 μm evaluated in 2 M H_2SO_4 solution. D) The changes of impedance value of various scaffolds consisting of 0-5 wt.% Gr nanosheets at frequency=20 Hz revealed the presence of a crucial point in which the electrical conductivity was the best. The schematic of the percolation theory revealed that the presence of a crucial point between 0.5-2 in which the broad conductive path was formed through the bridging Gr nanosheets (the red line).

Fig. 4. Mechanical properties of fibrous samples consisting of various amounts of Gr nanosheets; A) The representative image of 1Gr-AP scaffold (i) before and (ii) during the tensile loading. Hybrid 1Gr-AP fibrous scaffold exhibited resistance to fracture at high strain during uniaxial tensile test (148%). B) Representative uniaxial tensile stress-strain plots of crosslinked nanofibrous scaffolds after 1 days soaking in PBS. C) Schematic illustrating the formation of the interpenetrating network of PVA:SA, via physical crosslinking of PVA by heat treatment and chemical crosslinking of Alginate by CaCl2 solution, as well as the hydrogen bonding between Gr nanosheets and polymer matrix leading to significantly promoted mechanical properties. D) Comparison of the elastic moduli and toughness for previously reported compliant fibrous scaffolds (open circle) [41, 63-69] and the proposed Gr-AP scaffolds in hydrated state. The dashed window demonstrates the area with the best mechanical properties for nerve tissue engineering. Black arrow revealed that the toughness of AP fibrous scaffolds noticeably promoted via incorporation of 1 wt.% Gr nanosheets

Fig. 5. PC12 attachment on the various fibrous scaffolds; SEM images of PC12 cells after 1 day of culture on A) AP, B) 0.5Gr-AP, C) 1Gr-AP, D) 2Gr-AP and E) 5Gr-AP fibrous scaffolds. Red arrows show the formation of cell colony and its distribution. E) Cell retention, the fraction of

area covered with cell clusters, on the fibrous scaffolds. Cell spreading significantly enhanced on 1Gr-AP and 2Gr-AP scaffolds compared to others. (* $P < 0.05$).

Fig. 6. PC12 spreading on the various fibrous scaffolds; SEM images of PC12 cells after 7 days of culture on A) AP, B) 0.5Gr-AP, C) 1Gr-AP, D) 2Gr-AP and E) 5Gr-AP fibrous scaffolds. Red arrows show the distribution and spreading of PC12 cells. E) Cell spreading, the fraction of area covered with cell clusters, on the fibrous scaffolds. Cell spreading significantly enhanced on 1Gr-AP and 2Gr-AP scaffolds compared to others. (* $P < 0.05$).

Fig. 7. Cell viability of PC12 on various fibrous scaffolds measured using MTT assays after 3 and 7 days of culture. The absorbance was normalized against the control (TCP) at each time interval. (*$P < 0.05$).

ACCEPTED MANUSCRIPT